Performance Limits for Filtered Multitone Modulation in Fading Channels

Andrea M. Tonello, *Member, IEEE*

***Abstract*—In this paper, we investigate the best attainable performance for filtered multitone modulation (FMT) in time-variant frequency-selective fading channels when optimal maximum-likelihood (ML) detection is deployed. FMT generalizes the popular orthogonal frequency division multiplexing (OFDM) scheme through the deployment of subchannel shaping filters. The performance limits are derived by extending to this multichannel context the matched filter bounding technique. We first conduct an exact calculation for the average and the distribution of the matched filter error rate bound. Then, we follow a numerical procedure that overcomes the problems of accuracy and ill conditioning in the implementation of the exact method. This study allows for an analytical treatment of the diversity effect on performance as a function of the time/frequency selectivity of the channel. It is found that FMT is a diversity transform that is capable of yielding coding gains and time/frequency diversity gains as a function of the subcarrier spacing and the subchannel filter shape.**

***Index Terms*—Diversity, fading channels, filtered multitone modulation (FMT), matched filter bound, multicarrier modulation, OFDM, optimal detection.**

I. Introduction

In this paper, we investigate the performance limits for multicarrier (MC) modulation over time-variant frequency-selective fading channels. The basic principle behind MC modulation is to convert a sequence of data symbols at high rate into a number of subsequences at low rate [4], [30]. Each low rate sequence is transmitted through a subchannel that is shaped with an appropriate filter centered on a given subcarrier. When the subcarriers are uniformly spaced and the subchannel filters are identical, an efficient digital implementation is possible and is generally referred to as filtered multitone modulation (FMT) [7]. It is based on a fast Fourier transform (FFT) followed by low rate subchannel filtering. Discrete multitone modulation (DMT) is a particular implementation that deploys rectangular time-domain filters. DMT is also referred to as orthogonal frequency division multiplexing (OFDM) [4].

Channel frequency selectivity introduces intercarrier (ICI) and intersymbol (ISI) interference at the receiver [7]. The design of the subchannel filters and the choice of the subcarrier spacing in an FMT system aim at subdividing the spectrum into a number of subchannels that do not overlap in the frequency domain such that we can avoid the ICI and get low ISI contributions. In a DMT system, the insertion of a cyclic prefix longer than the channel time dispersion is such that ISI and ICI are eliminated and the receiver simplifies to a simple one-tap equalizer per subchannel. Clearly, the insertion of the cyclic prefix as well as an increase of the subcarrier spacing translates into a data rate penalty. The channel temporal selectivity can also introduce ICI as a result of loss of subchannel orthogonality [17], [21]. This happens when the channel is not static over the duration of the subchannel pulse.

The presence of ISI and ICI is such that some form of multichannel equalization is required [3], [7], [21]–[24]. The optimal receiver searches for the maximum-likelihood (ML) solution by implementing a multichannel Viterbi algorithm with an appropriate metric. The optimal FMT detector herein described is an extension of Ungerboeck's single-channel equalizer [28] and van Etten's multichannel equalizer [29]. It has some similarity with the ML sequence estimator (MLSE)/maximum *a posteriori* (MAP) equalizer for space–time coded systems that we describe in [25].

For uncoded transmission, a limit (lower bound) on the attainable performance is given by the probability of error achieved with ideal equalization, i.e., matched filter performance bound (MFB). That is, the bit-error rate (BER) achieved when the ML receiver is capable of canceling all interference components. The analysis of the MFB has attracted considerable attention since it allows for an analytical treatment of the diversity effect on performance as a function of the channel time and frequency selectivity. Mazo has studied the exact MFB for two-beam static Rayleigh fading [13]. Clark *et al.* have evaluated the MFB in static frequency-selective Rayleigh fading with (spatial) diversity combining receivers [8]. Schlegel has considered the multibeam static Rayleigh fading channel [15]. More recently, [1] and [11] have extended the study to doubly (time–frequency) dispersive channels. In [1], [8], and [11], the derivation of the average MFB error rate, taken over the ensemble of channel responses, starts from the Karhunen–Loève expansion of the received pulse.

In this paper, we study the MFB performance of uncoded FMT modulation. First, we develop an equivalent discrete-time doubly dispersive channel model. This is followed by the derivation of the distribution of the squared distance that is associated with a pairwise single error event. Such a distribution is obtained through the residues method of a normal quadratic form [5], [15]. Unfortunately, the residues method becomes numerically inaccurate and ill conditioned in the presence of

Manuscript received April 15, 2003; revised February 2, 2004; accepted June 16, 2004. The editor coordinating the review of this paper and approving it for publication is D. Gesbert. Part of this work was presented at the IEEE Wireless Personal Multimedia Communications (WPMC) Symposium 2002, Honolulu, HI, October 2002, and at the WPMC Symposium 2003, Yokosuka, Japan, October 2003.

The author is with the Dipartimento di Ingegneria Elettrica, Gestionale e Meccanica, Università di Udine, 33100 Udine, Italy (e-mail: tonello@uniud.it).

Digital Object Identifier 10.1109/TWC.2005.853872

multiple poles. To overcome such a problem, we also evaluate the average probability of error with a numerical method based on a Gauss–Chebyshev quadrature rule that has recently been presented in [19].

Our study includes the effect of the prototype pulse, the number of tones, the digital-to-analog and analog-to-digital converter (DAC and ADC) filters, as well as the impact on performance of the channel time–frequency selectivity. The MFB analysis reveals that FMT modulation can be interpreted as a diversity transform. When optimally detected, FMT modulation is capable of yielding coding and diversity gains as a function of the subchannel filter impulse response, the number of tones, and the time–frequency characteristics of the channel. In general, an increase in the number of subcarriers translates into a loss of achievable frequency diversity gain but into an increase in the time diversity gain.

This paper is organized as follows. In Section II, we describe the discrete-time transmission model, review the optimal ML FMT detector, and discuss some implications about complexity. In Section III, we carry out the performance analysis. An analysis of the effect of channel frequency and temporal selectivity is reported in Section IV, where we also summarize some results on the performance of conventional detection of OFDM. Numerical results are reported in Section V. Finally, the conclusions follow. The notation used is summarized in the footnote.[1]

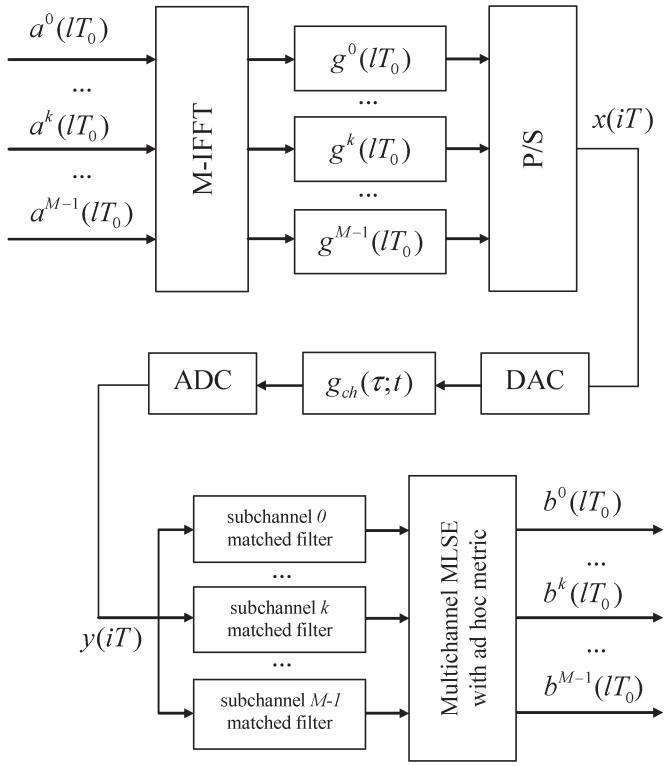

Fig. 1. FMT system with minimal subcarrier spacing (baseband representation).

II. Transmission and Reception Model With FMT

An MC-modulated signal (complex low-pass representation) can be written as

$$x(t) = \sum_{k\in\mathcal{K}} \sum_{l\in\mathbb{Z}} a^k(lT_0) g(t - lT_0) e^{j2\pi f_k t}, \qquad t \in \mathbb{R}; \quad \mathcal{K} = \{0, \ldots, M-1\} \quad (1)$$

where $a^k(lT_0)$ is the sequence of complex data symbols, e.g., belonging to M-quadrature-amplitude modulation (QAM) or M-phase-shift keying (PSK), transmitted on subchannel k at rate $1/T_0$ with $T_0 = NT$; $g(t)$ is a subchannel shaping filter (prototype filter); and $\mathcal{K}$ is the set of subcarrier indices k. The subchannel carrier frequency is f_k, and in general $N \geq M$.

We consider a discrete-time implementation that is obtained by sampling (1) at rate $1/T$, which yields

$$x(iT) = \sum_{k\in\mathcal{K}} \sum_{l\in\mathbb{Z}} \tilde{a}^k(lT_0) g_T^k(iT - lT_0) \qquad i \in \mathbb{Z} \quad (2)$$

when we define the subchannel transmit filter as $g_T^k(t) = g(t)e^{j2\pi f_k t}$ (frequency shifted prototype pulse) and $\tilde{a}^k(lT_0) = e^{j2\pi f_k lT_0} a^k(lT_0)$. An efficient implementation, referred to as FMT, is possible when the subcarriers are uniformly spaced, i.e., $f_k = k/T_1$ with $T_1 = MT$. It comprises the S/P conversion of the data symbol stream, an M-point inverse FFT (IFFT), and low-rate subchannel (polyphase) filtering [7]. This implementation is depicted in Fig. 1, where we assume minimal subcarrier spacing (critically sampled FMT system) and, therefore, we can set $N = M$, $\tilde{a}^k(lT_0) = a^k(lT_0)$, and $g^k(lT_0) = g(kT + lT_0)$.

The subchannel has nominal bandwidth $1/T_0 \leq 1/T_1$ that, for fixed T, becomes smaller as the number of subcarriers increases. With a sufficiently high number of subcarriers, the unfolded spectrum of (2) has width almost entirely confined in $W = 1/T$. This can be practically achieved by avoiding transmission over some of the outermost subcarriers. As an example, we consider the deployment of rectangular time-domain prototype pulses, rectangular frequency domain pulses, and Gaussian pulses

$$g_{\text{rect}}(i) = g_{\text{rect}}(iT) = \frac{1}{\sqrt{N}} \text{rect}\left(\frac{i}{N}\right)$$

$$g_{\text{sinc}}(i) = \frac{1}{\sqrt{N}} \text{sinc}\left(\frac{i}{N}\right)$$

$$g_{\text{gauss}}(i) = \sqrt{\frac{\sigma}{N}} \sqrt[4]{\frac{2}{\pi}} e^{-\left(\frac{\sigma i}{N}\right)^2} \quad (3)$$

[1]**Notation**. $\mathbf{a}$ denotes a column vector. $\mathbf{A}$ denotes a matrix. * denotes conjugation. $^{\mathrm{T}}$ denotes transposition. $^{\mathrm{H}}$ denotes conjugate transposition. $|\mathbf{A}|$ is the determinant of $\mathbf{A}$. $\text{rank}\{\mathbf{A}\}$ is the rank of matrix $\mathbf{A}$. $\text{diag}\{\mathbf{a}\}$ is a diagonal matrix with diagonal elements given by $\mathbf{a}$. $\text{diag}\{\mathbf{A}, \mathbf{B}, \ldots\}$ is a block diagonal matrix with blocks given by $\mathbf{A}, \mathbf{B}, \ldots$. $\text{toepz}\{\mathbf{a}\}$ is the Hermitian Toeplitz matrix with the first row equal to $\mathbf{a}^{\mathrm{T}}$. $\text{toepz}\{\mathbf{A}_0, \mathbf{A}_1, \ldots\}$, with $\mathbf{A}_i$ square matrix of size N, denotes a block Hermitian Toeplitz matrix with the first row of blocks equal to $\mathbf{A}_0, \mathbf{A}_1, \ldots$. The integer division and the remainder of the integer division are denoted as $a \text{ div } b$ and $a \bmod b$. $\text{Re}\{\cdot\}$ denotes the real part. $G(f) = \mathcal{F}\{g(t)\}$ is the Fourier transform of $g(t)$. $rep_{1/T}\{G(f)\}$ is the periodic repetition with rate $1/T$ of $G(f)$. j is the imaginary unit. $Q(x) = 1/\sqrt{2\pi}\int_x^\infty e^{-t^2/2}dt$ is the Q-function. $1(t)$ is the step-function. $\text{rect}(i/N) = 1$ for $i \in [0, N-1]$ and 0 otherwise. $\text{sinc}(i) = \sin(\pi i)/(\pi i)$.

where $\sigma = B\pi\sqrt{2/\ln 2}$ and $B = f_{3\text{-dB}}T_0$ is the normalized bandwidth. Note that the Gaussian pulses have the interesting property of having concentrated impulse and frequency response.

A. Discrete-Time Channel Model

The MT signal (2) is digital-to-analog converted, modulated to radio frequency (RF), and transmitted over the air. The received signal is RF demodulated and analog-to-digital converted (Fig. 1). Let $g_{ch}(\tau;t)$ be the baseband impulse response of the time-variant fading channel. The concatenation of the filters in the DAC, the channel, and the filter in the ADC has a time-variant impulse response $h_E(\tau;t)/T$. If we assume the channel to be practically time invariant over the duration of the ADC filter whose main lobe has duration $\sim 2T$, we can approximate it as

$$h_E(\tau;t) \approx \int_{\mathbb{R}} g_{ch}(\tau_1;t) g_B(\tau-\tau_1)\mathrm{d}\tau_1 \tag{4}$$

with $g_B(\tau) = \int_{\mathbb{R}} g_{\mathrm{ADC}}(\tau_1) g_{\mathrm{DAC}}(\tau-\tau_1)\mathrm{d}\tau_1$ [21]. Conventionally, the analog filters in the DAC and ADC are square-root-raised cosine filters with Nyquist frequency $0.5/T$. Thus, the sequence of received samples at rate $1/T$ (assuming exact sampling phase) can be written as

$$y(iT) = \sum_{n\in\mathbb{Z}} x(nT) h_E(iT-nT;iT) + w(iT) \tag{5}$$

where $w(iT)$ is a sequence of independent identically distributed (i.i.d.) circularly symmetric complex Gaussian random variables with zero-mean and variance N_0. Note that with the above assumptions, the channel is not necessarily static over the duration of the prototype pulse. If we define the equivalent subchannel receive filter as

$$g_R^k(\tau;t) = \sum_{i\in\mathbb{Z}} g_T^k(iT) h_E(\tau-iT;t) \tag{6}$$

the broadband received signal can be written as the superposition of M narrowband signals

$$y(iT) = \sum_{k\in\mathcal{K}} \sum_{l\in\mathbb{Z}} \tilde{a}^k(lT_0) g_R^k(iT-lT_0;iT) + w(iT). \tag{7}$$

If we assume wide sense stationary uncorrelated scattering (WSSUS) and a common time selective correlation function across the delay profile [1], [2], [10], the channel is a zero mean complex Gaussian process with autocorrelation

$$\begin{aligned} r_g(\tau_1,\tau_2;t_1,t_2) &= E\left[g_{ch}(\tau_1;t_1) g_{ch}^*(\tau_2;t_2)\right] \\ &= \phi_g(\tau_1)\psi_d(t_2-t_1)\delta(\tau_2-\tau_1) \end{aligned} \tag{8}$$

where $\phi_g(\tau)$ denotes the delay power spectrum while $\psi_d(t)$ denotes the time-selective correlation function. In the literature, several models are available to represent the delay power spectrum, for instance, the one-sided exponential model, or the Gaussian model [6], [8]. Impulsive models are also used, for instance, the Third Generation Partnership Project-International Telecommunication Union (3GPP-ITU) channel models [12]. For the Doppler spectrum, we use the Jakes' model that is derived under the assumption of isotropic scattering [10]. For this model, $\psi_d(t) = J_0(2\pi f_D t)$, where $J_0(t)$ denotes the zero-order Bessel function of the first kind and f_D is the one-sided Doppler spread. It follows that

$$\begin{aligned} &r_h(\tau_1,\tau_2;t_1,t_2) \\ &\quad = E\left[h_E(\tau_1;t_1) h_E^*(\tau_2;t_2)\right] \\ &\quad = J_0\left(2\pi f_D(t_2-t_1)\right) \\ &\qquad \times \int_{\mathbb{R}} \phi_g(\tau_3) g_B(\tau_1-\tau_3) g_B^*(\tau_2-\tau_3)\mathrm{d}\tau_3. \end{aligned} \tag{9}$$

We can represent the discrete-time channel impulse response with a T-spaced tapped delay line

$$h_E(nT;iT) = \sum_{p\in\mathcal{P}} \alpha_p(iT)\delta(nT-pT), \qquad \mathcal{P} = \{-N_P,\ldots,N_P\} \tag{10}$$

that has Gaussian-distributed tap gains with correlation $E[\alpha_{p_1}(i_1T)\alpha_{p_2}^*(i_2T)] = r_h(p_1T,p_2T;i_1T,i_2T)$.

Throughout this paper, we use matrix notation.[1] In particular, we denote the channel taps mean vector as $\mathbf{m} = E[\boldsymbol{\alpha}]$ and the correlation matrix as $\mathbf{R} = E[\boldsymbol{\alpha}\boldsymbol{\alpha}^{\mathrm{H}}]$, where the vector $\boldsymbol{\alpha}$ is defined as

$$\boldsymbol{\alpha} = \left[\boldsymbol{\alpha}_{-L}^{\mathrm{T}},\ldots,\boldsymbol{\alpha}_L^{\mathrm{T}}\right]^{\mathrm{T}}, \quad \boldsymbol{\alpha}_i = \left[\alpha_{-N_P}(iT),\ldots,\alpha_{N_P}(iT)\right]^{\mathrm{T}} \tag{11}$$

for given integers N_P, L, and $i = -L,\ldots,L$. The correlation matrix is Hermitian, with size $(2N_P+1)(2L+1)$, and with elements $r_h(p_1T,p_2T;i_1T,i_2T)$. To proceed further, if we use the numerical integration of (9), we can write

$$\begin{aligned} r_h(p_1T,p_2T;i_1T,i_2T) &= J_0\left(2\pi f_D(i_2-i_1)T\right) \\ &\quad \times \sum_{l=-N_L}^{N_L} \phi_l g_B(p_1T-lT_c) g_B^*(p_2T-lT_c) \end{aligned} \tag{12}$$

with $\phi_l = T_c\phi_g(lT_c)$, $T_c = T/K$, and $K \geq 1$. Then, in matrix notation, we have

$$\mathbf{R} = E[\boldsymbol{\alpha}\boldsymbol{\alpha}^{\mathrm{H}}] = \mathrm{toepz}\left\{\mathbf{G}_B^{\mathrm{H}}\boldsymbol{\Phi}_0\mathbf{G}_B,\ldots,\mathbf{G}_B^{\mathrm{H}}\boldsymbol{\Phi}_{2L}\mathbf{G}_B\right\} \tag{13}$$

$$\boldsymbol{\Phi}_i = J_0(2\pi f_D iT)\mathrm{diag}\left\{\phi_{-N_L},\ldots,\phi_{N_L}\right\} \tag{14}$$

$$\mathbf{G}_B = \begin{bmatrix} g_B(-N_PT+N_LT_c) & \ldots & g_B(N_PT+N_LT_c) \\ \ldots & \ldots & \ldots \\ g_B(-N_PT-N_LT_c) & \ldots & g_B(N_PT-N_LT_c) \end{bmatrix}. \tag{15}$$

B. Optimal Multitone Detection

The optimal multitone detector has been described in [21]–[24] for the more general multiuser context. For the scenario of this paper, it basically consists of a bidimensional

equalizer that deals with both the ICI and the ISI by implementing a Viterbi algorithm with an appropriate metric. Under certain conditions, it simplifies into a bank of single-channel Viterbi equalizers. This is shown in what follows.

Given the model in (7), the optimal ML detector seeks the data sequence $\mathbf{b} = \{b^k(lT_0)\}, l \in \mathbb{Z}, k \in \mathcal{K} = \{0, \ldots, M-1\}$, that minimizes the accumulated squared Euclidean distance $\Delta_e = \sum_{i\in\mathbb{Z}} |y(iT) - \sum_{l\in\mathbb{Z}} \sum_{k\in\mathcal{K}} \tilde{b}^k(lT_0)\, g_R^k(iT - lT_0; iT)|^2$. We can partition the accumulated distance as (neglecting a constant additive term)

$$\Delta_e \sim -\operatorname{Re}\left\{ \sum_{l\in\mathbb{Z}} \sum_{k\in\mathcal{K}} b^{k^*}(lT_0) e^{-j2\pi f_k l T_0} \times \left(2z^k(lT_0) - \sum_{l'\in\mathbb{Z}} \sum_{k'\in\mathcal{K}} b^{k'}(l'T_0) \times e^{j2\pi f_{k'} l' T_0} s^{k,k'}(l;l') \right) \right\} \quad (16)$$

$$z^k(lT_0) = \sum_{i\in\mathbb{Z}} y(iT) g_R^{k^*}(iT - lT_0; iT) \quad (17)$$

$$s^{k,k'}(l;l') = \sum_{i\in\mathbb{Z}} g_R^{k^*}(iT - lT_0; iT) g_R^{k'}(iT - l'T_0; iT). \quad (18)$$

Let us define the index relations $m = k + lM - 1$, $l(m) = m \text{ div } M$, and $k(m) = m \bmod M$, for $k = 0, \ldots, M-1$, $l, m \in \mathbb{Z}$. Then, the accumulated distance can be written as $\Delta_e \sim -\sum_{m\in\mathbb{Z}} \operatorname{Re}\{b_m^* [2z_m - \sum_{m'\in\mathbb{Z}} b_{m'} s_{m,m'}]\}$, where $b_m = b^{k(m)}(l(m)T_0) e^{j2\pi f_{k(m)} l(m) T_0}$, $z_m = z^{k(m)}(l(m)T_0)$, and $s_{m,m'} = s^{k(m),k(m')}(l(m); l(m'))$.

Since $s_{m,m'} = s_{m',m}^*$, we can finally rewrite (16) as

$$\Delta_e \sim -\sum_{m\in\mathbb{Z}} \operatorname{Re}\left\{ b_m^* \left(2z_m - b_m s_{m,m} - 2\sum_{m'>0} b_{m-m'} s_{m,m-m'} \right) \right\}. \quad (19)$$

Therefore, the search for the ML transmitted sequence can be implemented with a Viterbi algorithm [14]. The search algorithm sequentially processes the z-parameters (17) (subchannel matched filter outputs).

Using (10), the s-parameters (18) can be written as

$$s^{k,k'}(l;l') = \sum_{i\in\mathbb{Z}} \sum_{p,p'\in\mathcal{P}} \Big(\alpha_p^*(iT) \alpha_{p'}(iT) g_T^{k^*}(iT - lT_0 - pT) \times g_T^{k'}(iT - l'T_0 - p'T) \Big). \quad (20)$$

Their computation requires knowledge of the time-variant channel taps or of the equivalent subchannel impulse responses. The s-parameters correspond to the subchannel cross correlations, and therefore, they give the ISI and ICI weight components as a function of the propagation conditions and the subchannel transmission pulse.

The complexity of the optimal detector is determined by the number of states in the Viterbi algorithm that is equal to C^J, where C denotes the constellation size and J is an integer such that $s_{m,m-m'} = 0$ for $m' > J$. The memory J, and therefore the algorithm complexity, is a function of both the channel and the prototype pulse as we illustrate in the next two examples.

If we assume a static channel that does not vary over the duration of the detection frame, i.e., $\alpha_p(iT) = \alpha_p$, using Parseval's theorem, (20) can be rewritten as

$$s^{k,k'}(l;l') = T^{-1} \sum_{p,p'\in\mathcal{P}} \alpha_p^* \alpha_{p'} \times \int_{-0.5/T}^{0.5/T} \operatorname{rep}_{\frac{1}{T}} \left\{ G^*(f - f_k) e^{j2\pi f(lT_0 + pT)} \right\} \times \operatorname{rep}_{\frac{1}{T}} \left\{ G(f - f_{k'}) e^{-j2\pi f(l'T_0 + p'T)} \right\} \mathrm{d}f \quad (21)$$

where $G(f) = \mathcal{F}\{g(t)\}$ with $t, f \in \mathbb{R}$. If the subchannel filters are band limited with a bandwidth smaller than the subcarrier spacing, the s-parameters are zero for $k \neq k'$. Therefore, the multichannel detector simplifies into M single-channel ML detectors that have to deal with the ISI only. With sinc pulses (ideal FMT), the condition is met. With rect pulses (DMT), the ICI interference is high, which increases the complexity of the optimal detector. In the latter case, simplified detection is possible when deploying a cyclic prefix, see Section IV-C.

If we assume a time-variant single tap channel, (20) can be rewritten as

$$s^{k,k'}(l;l') = e^{j2\pi(f_k l T_0 - f_{k'} l' T_0)} \times \sum_{i\in\mathbb{Z}} e^{j2\pi(f_{k'} - f_k) iT} |\alpha(iT)|^2 g^*(iT - lT_0) g(iT - l'T_0). \quad (22)$$

If the prototype filter has a duration smaller than T_0, the s-parameters are zero for $l \neq l'$, while for $l = l'$, $s^{k,k'}(l;l) = \sum_i e^{j2\pi(f_{k'} - f_k) iT} |\alpha(iT)|^2 |g(iT - lT_0)|^2$. With rect pulses, the condition is met; therefore, a time-variant channel does not introduce ISI. However, ICI is present such that the optimal detector must jointly detect all subchannels. With sinc pulses, the complexity grows even more because ISI also exists.

To minimize the amount of ICI and ISI, and keep the detection complexity at low levels, it is desirable to use time and frequency concentrated pulses, e.g., Gaussian-shaped pulses [24]. In the next sections, we study how the design parameters (prototype pulse and number of tones) impact performance.

III. Performance Limits of Optimal MT Detection

Under the hypothesis of perfect knowledge of the channel state information $\mathbf{s}$ (s-parameters), the pairwise error probability (PEP), i.e., the probability that the optimal MT detector

decides erroneously in favor of the sequence $\mathbf{b} = \{b^k(lT_0)\}$, $k \in \mathcal{K}$, $l \in \mathbb{Z}$, when $\mathbf{a} = \{a^k(lT_0)\}$ was transmitted, is given by

$$P(\mathbf{a} \to \mathbf{b}|\mathbf{s}) = Q\left(\sqrt{\frac{d^2(\mathbf{a},\mathbf{b})}{2N_0}}\right) \tag{23}$$

where the pairwise error event squared distance is

$$d^2(\mathbf{a},\mathbf{b}) = \sum_{i\in\mathbb{Z}} \left| \sum_{l\in\mathbb{Z}} \sum_{k\in\mathcal{K}} e^k(lT_0) g_R^k(iT - lT_0; iT) \right|^2 \tag{24}$$

$$e^k(lT_0) = e^{j2\pi f_k lT_0} \left(a^k(lT_0) - b^k(lT_0)\right). \tag{25}$$

Using the s-parameter definition, we obtain

$$d^2(\mathbf{a},\mathbf{b}) = \sum_{l,l'\in\mathbb{Z}} \sum_{k,k'\in\mathcal{K}} e^{k^*}(lT_0) e^{k'}(l'T_0) s^{k,k'}(l;l'). \tag{26}$$

The average (over the ensemble of channel responses) PEP is the result of the expectation

$$P(\mathbf{a} \to \mathbf{b}) = E\left[Q\left(\sqrt{\frac{d^2(\mathbf{a},\mathbf{b})}{2N_0}}\right)\right]. \tag{27}$$

Starting from (27), in what follows we derive error probability limits for uncoded transmission. For uncoded transmission, single error events are possible such that the detected sequence may differ only in one data symbol from the transmitted sequence. In the literature, the corresponding PEP is referred to as the MFB [1], [8], [11]. The MFB represents a performance limit (lower bound) that can be achieved with perfect equalization, i.e., when the ML receiver cancels all interference components or equivalently when a single isolated pulse is transmitted. Assuming i.i.d. equiprobable binary PSK (BPSK) or quaternary PSK (QPSK) data symbols, the MFB yields a lower bound to the bit error probability of the ML detector.

Let us assume the single error event $e^k(lT_0)$ to occur on subchannel k and at time instant lT_0. Then, the error event distance (26) can be written as

$$\begin{aligned} d^2_{\mathrm{MFB}}(k,l) &= D_e s^{k,k}(l;l) \\ &= D_e \sum_{i\in\mathbb{Z}} \sum_{p,p'\in\mathcal{P}} \Big(\alpha_p^*(iT + lT_0)\alpha_{p'}(iT + lT_0) \\ &\quad \times e^{j2\pi f_k(pT - p'T)} g^*(iT - pT) g(iT - p'T) \Big) \end{aligned} \tag{28}$$

where $D_e = |e^k(lT_0)|^2$ is the squared Euclidean distance between the transmitted and the detected data symbol. For BPSK signaling, $D_e = 4E_S$ with E_S equal to the average symbol energy. In general, (28) is a function of the subchannel index, the time instant, and the symbol error event.

To proceed, let us assume the channel response and the prototype pulse to have (practically) finite duration. Then, $\mathcal{P} = \{-N_P, \ldots, N_P\}$ and $g(iT) = 0$ for $i \notin \{-N_g, \ldots, N_g\}$. Setting $L = N_g + N_P$, with matrix notation we obtain

$$\begin{aligned} d^2_{\mathrm{MFB}}(k,l) &= D_e \sum_{i\in\mathbb{Z}} \boldsymbol{\alpha}^{\mathrm{H}}_{i+lN} \mathbf{W}^{\mathrm{H}}_{k,0} \mathbf{G}_i \mathbf{W}_{k,0} \boldsymbol{\alpha}_{i+lN} \\ &= \boldsymbol{\alpha}^{\mathrm{H}} \mathbf{W}^{\mathrm{H}}_k \mathbf{G} \mathbf{W}_k \boldsymbol{\alpha} \end{aligned} \tag{29}$$

where $\boldsymbol{\alpha}$ is defined in (11) and

$$\begin{aligned} \mathbf{g}_i &= [g(iT + N_P T), \ldots, g(iT - N_P T)]^{\mathrm{T}} \\ \mathbf{G}_i &= \mathbf{g}_i^* \mathbf{g}_i^{\mathrm{T}}, \quad i = -L, \ldots, L \\ \mathbf{G} &= \mathrm{diag}\{\mathbf{G}_{-L}, \ldots, \mathbf{G}_L\} \\ \mathbf{W}_{k,0} &= \mathrm{diag}\{e^{-j2\pi f_k N_P T}, \ldots, e^{j2\pi f_k N_P T}\} \\ \mathbf{W}_k &= \mathrm{diag}\{\underbrace{\mathbf{W}_{k,0}, \ldots, \mathbf{W}_{k,0}}_{2L+1}\}. \end{aligned} \tag{30}$$

Since the vector of channel taps $\boldsymbol{\alpha}$ is Gaussian, (29) is a normal quadratic form [9], [16] (see Appendix A).

We note that when the channel impulse response is sparse, it is possible to reduce the size of the vectors and matrices in (29). That is, we can write $d^2_{\mathrm{MFB}}(k,l) = D_e \widehat{\boldsymbol{\alpha}}^{\mathrm{H}} \widehat{\mathbf{W}}^{\mathrm{H}}_k \widehat{\mathbf{G}} \widehat{\mathbf{W}}_k \widehat{\boldsymbol{\alpha}}$, where $\widehat{\boldsymbol{\alpha}}$ is obtained by deleting the zero components of $\boldsymbol{\alpha}$, while $\widehat{\mathbf{G}}$ and $\widehat{\mathbf{W}}_k$ are obtained by deleting the rows and columns with indices corresponding to the zero elements of $\boldsymbol{\alpha}$.

In the following sections, we evaluate the MFB error probability in Rayleigh fading by applying three methods. The first is based on the application of the residues method where the probability density function (pdf) of the quadratic form (29) is computed in closed form. In the second approach, we follow a recently proposed numerical method to compute the expectation (27). Finally, we study the Chernoff bound.

A. Residues Method and Gauss–Chebyshev Numerical Quadrature Method

Assuming the channel taps to be zero mean circularly symmetric complex Gaussian (Rayleigh fading), (29) is a central normal quadratic form [5], [15], [16]. Let $\mathbf{R} = E[\boldsymbol{\alpha}\boldsymbol{\alpha}^{\mathrm{H}}]$ be the channel correlation matrix that we assume to be full rank. Although not explicitly shown for ease of notation, we assume the reduced size vectors that are obtained through deletion of the zero components of $\boldsymbol{\alpha}$ (see previous section). Using some results on quadratic forms that are summarized in Appendix A, the squared MFB distance can be rewritten as

$$d^2_{\mathrm{MFB}}(k) = \sum_{i=1}^{N_\lambda} \lambda_i |\beta_i|^2 \tag{31}$$

where λ_i are the N_λ eigenvalues of the matrix $D_e \mathbf{R} \hat{\mathbf{G}}_k$ with $\hat{\mathbf{G}}_k = \mathbf{W}^{\mathrm{H}}_k \mathbf{G} \mathbf{W}_k$ and β_i are i.i.d. complex Gaussian random variables with zero mean and unit variance. Note that we have dropped the dependency on l since we assume to be in stationary conditions.

The pdf $p_{d^2_{\mathrm{MFB}}}(a)$ and the probability distribution function $F_{d^2_{\mathrm{MFB}}}(a)$ of (31) can be found through the inversion of the

characteristic function (see Appendix A). Let us assume that we have N' out of N_λ distinct eigenvalues $\lambda_1, \ldots, \lambda_{N'}$, each with multiplicity $m_1, \ldots, m_{N'}$, then

$$p_{d^2_{\mathrm{MFB}}}(a) = \sum_{i=1}^{N'} \sum_{n=1}^{m_i} A_{i,n} \frac{a^{n-1}}{\lambda_i^n (n-1)!} e^{-\frac{a}{\lambda_i}}, \quad a \geq 0 \tag{32}$$

$$F_{d^2_{\mathrm{MFB}}}(a) = \sum_{i=1}^{N'} \sum_{n=1}^{m_i} A_{i,n} \left(1 - e^{-\frac{a}{\lambda_i}} \sum_{l=0}^{n-1} \left(\frac{a}{\lambda_i}\right)^l \frac{1}{l!}\right), \quad a \geq 0 \tag{33}$$

where $A_{i,n}$ are the coefficients of the partial fraction expansion of the characteristic function (residues)[2]

$$A_{i,n} = \frac{1}{(-\lambda_i)^{m_i - n}(m_i - n)!} \times \left[\frac{d^{m_i-n}}{ds^{m_i-n}} \left\{\prod_{p=1, p\neq i}^{N'} (1 - \lambda_p s)^{-m_p}\right\}\right]_{s=\frac{1}{\lambda_i}}. \tag{34}$$

It follows that the distribution of the squared distance is a weighed sum of Erlang distributions.

Now, the average matched filter probability of error bound is computed as $P_{e,\mathrm{MFB}} = \int_{R^+} Q(\sqrt{a/(2N_0)}) p_{d^2_{\mathrm{MFB}}}(a)\mathrm{d}a$. The integral can be evaluated in closed form (e.g., see [8]) yielding

$$P_{e,\mathrm{MFB}}(k) = \frac{1}{2} \sum_{i=1}^{N'} \sum_{n=1}^{m_i} A_{i,n} \times \left[1 - \sum_{l=0}^{n-1} \frac{(2l)!}{2^{2l}(l!)^2} \sqrt{\frac{\frac{\lambda_i}{4N_0}}{\left(1 + \frac{\lambda_i}{4N_0}\right)^{2l+1}}}\right]. \tag{35}$$

For BPSK and QPSK signaling, the matched filter BER bound on subcarrier k, $\mathrm{BER}(k)$, is given by (35) when D_e is, respectively, set to $D_e = 4E_S$ and $D_e = 2E_S$. Further, the BER complementary distribution equals (33)

$$P\left[\mathrm{BER}(k) \geq Q\left(\sqrt{\frac{a_0}{2N_0}}\right)\right] = F_{d^2_{\mathrm{MFB}}}(a_0). \tag{36}$$

The average (across subchannels) BER can be defined as

$$\mathrm{BER} = \frac{1}{M} \sum_{k \in \mathcal{K}} \mathrm{BER}(k). \tag{37}$$

The analysis is sufficiently general to be applied to higher-order constellations, e.g., M-QAM. We report numerical results corresponding to (35)–(37) for various transmission scenarios in Section V.

In the presence of multiple eigenvalues [poles of the characteristic function of (31)], accurate computation of the residues (34) becomes a numerically ill-posed problem [19]. A possible way to circumvent it is to calculate the pdf (32) through the FFT of the product form of the characteristic function (Appendix A). Then, the distribution and the average error probability are obtained using numerical integration. Alternatively, in [19], it is proposed to numerically evaluate expectations of the form $E[Q(\sqrt{\xi})]$ through a procedure that involves the computation of the moment generating function $\Phi_\Delta(s) = E[e^{-s\Delta}]$ of the random variable $\Delta = \xi - \nu^2$ with ν as a zero-mean unit-variance Gaussian and ξ a nonnegative random variable independent of ν. Then, through the application of a Gauss–Chebyshev numerical quadrature rule with w nodes, we obtain

$$P_{e,\mathrm{MFB}}(k) = E\left[Q(\sqrt{\xi})\right] = \frac{1}{4w} \sum_{n=1}^{w} (\mathrm{Re}\left\{\Phi_\Delta\left(c(1+j\tau_n)\right)\right\} + \tau_n \mathrm{Im}\left\{\Phi_\Delta(c(1+j\tau_n))\right\}) + E_w \tag{38}$$

with $0 < c < 1/2$ and $\tau_n = \tan((n - 0.5)\pi/w)$. The error E_w goes to zero as the number of nodes w goes to infinity. Details on the computation of $\Phi_\Delta(s)$ when $\xi = d^2_{\mathrm{MFB}}/(2N_0)$ can be found in Appendix B.

B. Gaussian Tail Function Bound

To get further physical insight, we study the Chernoff bound on (27). The Gaussian tail probability can be bounded as $Q(a) \leq 0.5e^{-a^2/2}$ [14]. Thus, we can write $P_{e,\mathrm{MFB}}(k) \leq 0.5 \exp(-1/(4N_0) \sum_{i=1}^{N_\lambda} \lambda_i |\beta_i|^2)$. Then, averaging over the distributions of $|\beta_i|^2$ (exponential), we obtain

$$P_{e,\mathrm{MFB}}(k) \leq \frac{1}{2} \prod_{i=1}^{N_\lambda} \left(1 + \frac{\lambda_i}{4N_0}\right)^{-1} \leq \frac{1}{2} \left(\frac{E_S}{4N_0}\right)^{-d} \prod_{\lambda_i \neq 0} \left(\frac{\lambda_i}{E_S}\right)^{-1} \tag{39}$$

where d equals the number of nonzero eigenvalues. This upper bound is useful to understand how the subchannel filter and the subcarrier spacing impact the MFB performance. It reveals that FMT modulation can be interpreted as a diversity transform that performs subchannel time or spectrum spreading as a function of the prototype filter and the subcarrier spacing, and in particular as follows.

1) FMT modulation with optimal detection can provide both diversity gain and coding gain over uncoded single carrier transmission through a flat Rayleigh fading channel. The diversity gain d equals the number of nonzero eigenvalues of $D_e \mathbf{R} \hat{\mathbf{G}}_k$ with $\hat{\mathbf{G}}_k = \mathbf{W}_k^{\mathrm{H}} \mathbf{G} \mathbf{W}_k$, while the product of the nonzero eigenvalues gives the coding gain.
2) The diversity gain satisfies the bound $d \leq \min\{\mathrm{rank}(\mathbf{R}), \mathrm{rank}(\hat{\mathbf{G}}_k)\}$. If the channel is frequency selective but time invariant, then $1 \leq d \leq \widehat{N}_P$, where $\widehat{N}_P$ equals the number of nonzero T-spaced channel taps. If the channel is frequency nonselective but time variant, then $1 \leq d \leq \widehat{L}$ with $\widehat{L}T$ equal to the prototype pulse duration.

[2]Note that when there is a single eigenvalue with multiplicity m, the coefficients in (34) are all zero with the exception of $A_{1,m} = 1$. When there are N distinct eigenvalues, $A_{i,1} = \prod_{p=1, p\neq i}^{N} (1 - \lambda_p/\lambda_i)^{-1}$.

A detailed discussion is given in the next section; however, it is clear that subchannel bandwidth expansion potentially increases the frequency diversity gain while subchannel bandwidth compression (pulse duration expansion) increases the time diversity gain.

We note that the above conclusions are based on the MFB analysis. Nevertheless, several results from simulation in [21]–[24] show that near MFB performance is achievable by deploying practicable maximum-likelihood detection schemes that are based on iterative interference cancellation techniques. Finally, it is interesting to note that some analogy exists with the analysis of the Chernoff bound on the PEP in space–time coded systems [20]. However, in the system that we consider, the multitone transform acts as a code that takes place across subchannels and not across antennas.

IV. Discussion

In this section, we investigate the MFB probability of error assuming first a time-invariant frequency-selective channel and then a time-variant flat-fading channel. These are two major scenarios that can be considered representative, respectively, of wideband communications and narrowband communications. Further, we briefly review the performance of conventional detection of OFDM with cyclic prefix.

A. Time-Invariant Frequency-Selective Channel

In this section, we assume the channel to be time invariant but frequency selective. The vector of channel taps is independent of time and according to (11) is denoted as $\boldsymbol{\alpha}_0 = [\alpha_{-N_P}, \ldots, \alpha_{N_P}]^{\mathrm{T}}$. Thus, we can rewrite the squared error distance as

$$d^2_{\mathrm{MFB}}(k) = D_e \boldsymbol{\alpha}_0^{\mathrm{H}} \mathbf{W}_{k,0}^{\mathrm{H}} \boldsymbol{\kappa} \boldsymbol{W}_{k,0} \boldsymbol{\alpha}_0 = \sum_{i=1}^{2N_P+1} \lambda_i |\beta_i|^2 \quad (40)$$

where $\boldsymbol{\kappa} = \sum_i \mathbf{G}_i$ is the prototype pulse autocorrelation matrix[3] with elements $(\boldsymbol{\kappa})_{p,p'} = \kappa(p-p') = \sum_i g^*(iT) g(iT + pT - p'T)$, while $\mathbf{W}_{k,0}$ is defined in (30). The $2N_P+1$ eigenvalues λ_i in (40) are the ones associated with the matrix $D_e \mathbf{R} \mathbf{W}_{k,0}^{\mathrm{H}} \boldsymbol{\kappa} \mathbf{W}_{k,0}$, where $\mathbf{R} = E[\boldsymbol{\alpha}_0 \boldsymbol{\alpha}_0^{\mathrm{H}}] = \mathbf{G}_B^{\mathrm{H}} \boldsymbol{\Phi}_0 \mathbf{G}_B$. The achievable diversity gain equals the number of nonzero eigenvalues and is lower or equal to $2N_P+1$.

A first interesting observation is that when the T-spaced channel taps are uncorrelated, i.e., $\mathbf{R}$ is diagonal, the matched filter error rate bound is not a function of the subchannel index k. This is because the eigenvalues of $D_e \mathbf{R} \mathbf{W}_{k,0}^{\mathrm{H}} \boldsymbol{\kappa} \mathbf{W}_{k,0}$ are independent of the index k. On the contrary, when the channel taps are correlated, the error rate performance may differ across the subchannels. Since we consider uncorrelated scattering, $\boldsymbol{\Phi}_0$ is diagonal. Therefore, in our model, correlation among the T-spaced channel taps can be introduced by the DAC–ADC filters. The effect of these filters is included in the matrix $\mathbf{G}_B$ that is defined in (15).

In general, the above results show that performance depends on the prototype pulse and the number of subcarriers. As we will illustrate in the numerical examples of Section V, the matched filter bound reveals that when transmission is through a frequency-selective channel, we get diminished frequency diversity gains as the number of subcarriers increases, independently of the prototype pulse. In particular, when the number of subcarriers tends to infinity, the MFB performance tends to the error rate that is achieved in flat fading such that no frequency diversity is exploited. This can be proved by observing that the squared distance (40) becomes

$$d^2_{\mathrm{MFB},M=N\to\infty}(k) = D_e \boldsymbol{\alpha}_0^{\mathrm{H}} \mathbf{F}_k \boldsymbol{\alpha}_0 \quad (41)$$

where $\mathbf{F}_k = \mathrm{toepz}\{[1, e^{-j2\pi f_k T}, e^{-j2\pi f_k 2T}, \ldots, e^{-j2\pi f_k 2N_P T}]\}$ and $0 \le f_k < 1/T$. Since $\mathbf{F}_k$ has rank 1, the matrix $\mathbf{R}\mathbf{F}_k$ has a single nonzero eigenvalue equal to $\lambda(k) = \mathrm{trace}(\mathbf{R}\mathbf{F}_k) = \sum_{n,m\in\mathcal{P}} R_{n,m} e^{j2\pi f_k (m-n)T}$ with $R_{n,m} = E[\alpha_n \alpha_m^*]$. If the channel taps are uncorrelated, all subchannels exhibit the same MFB performance since $\overline{\lambda} = \mathrm{trace}(\mathbf{R}\mathbf{F}_k) = \mathrm{trace}(\mathbf{R}) = 1$ (with a normalized power delay profile). If the channel taps are correlated and the number of subcarriers tends to infinity, the average error rate becomes larger or equal to the error rate in flat fading. In fact, we have that $\sum_{k\in\mathcal{K}} P_e(\lambda(k))/M \ge P_e(\overline{\lambda})$ since $P_e(\cdot)$ is a convex function.

Another interesting situation is when we set $M = N = 1$, which corresponds to single carrier modulation. According to the model in (5), pulse shaping is implemented by the DAC filter. The squared distance becomes

$$d^2_{\mathrm{MFB},M=N=1}(k) = D_e \boldsymbol{\alpha}_0^{\mathrm{H}} \boldsymbol{\alpha}_0 = D_e \sum_{p\in\mathcal{P}} |\alpha_p|^2. \quad (42)$$

Therefore, the achievable diversity gain equals the rank of the matrix $D_e \mathbf{G}_B^{\mathrm{H}} \boldsymbol{\Phi}_0 \mathbf{G}_B$ and can be as large as the number of nonzero T-spaced channel taps.

B. Time-Variant Frequency-Nonselective Channel

If we assume the channel to be frequency nonselective (flat) but time variant, we obtain

$$\begin{aligned} d^2_{\mathrm{MFB}} &= D_e \sum_{i\in\mathbb{Z}} |\alpha(iT)|^2 \, |g(iT)|^2 \\ &= D_e \hat{\boldsymbol{\alpha}}^{\mathrm{H}} \hat{\mathbf{G}} \hat{\boldsymbol{\alpha}} = \sum_{i=1}^{2N_g+1} \lambda_i |\beta_i|^2 \end{aligned} \quad (43)$$

where λ_i are the eigenvalues of $D_e E[\hat{\boldsymbol{\alpha}} \hat{\boldsymbol{\alpha}}^{\mathrm{H}}] \hat{\mathbf{G}} = D_e \hat{\mathbf{R}} \hat{\mathbf{G}}$ with $\hat{\boldsymbol{\alpha}} = [\alpha(-N_g T), \ldots, \alpha(N_g T)]^{\mathrm{T}}$, $\hat{\mathbf{G}} = \mathrm{diag}\{|g(-N_g T)|^2, \ldots, |g(N_g T)|^2\}$. The squared distance is identical over all subchannels.

If the channel is fully uncorrelated (ergodic), we have $2N_g+1$ eigenvalues $\lambda_i = D_e |g(iT)|^2$. In particular, with a rect prototype pulse, we get one eigenvalue $\lambda_i = D_e/N$ with multiplicity N. It follows that an increase in the number of subcarriers translates into increased temporal diversity gains.

[3] With a rect, a sinc, or a Gaussian prototype pulse, the autocorrelation coefficient can be calculated in closed form, yielding: $\kappa_{\mathrm{rect}}(p) = 1 - |p|/N$ if $|p| \le N$, 0 otherwise, $\kappa_{\mathrm{sinc}}(p) = \mathrm{sinc}(p/N)$, $\kappa_{\mathrm{gauss}}(p) = \exp(-0.5(\sigma p/N)^2)$, where the last expression holds for $B/N \ll 1$.

If the number of subcarriers goes to infinity, the distribution (33) goes to $F_{d^2}(a) = 1(a - D_e)$, i.e., the squared distance becomes deterministic.[4] Thus, the probability of error tends to the probability of error in the absence of fading [additive white Gaussian noise, (AWGN) only].

With single carrier transmission, we can write $d^2_{\mathrm{MFB},M=N=1} = D_e|\alpha(0)|^2$; therefore, there is only one eigenvalue $\lambda = D_e$ and consequently there is no temporal diversity exploitation. Recall that we have assumed the channel to be static over the duration of the ADC filter.

C. DMT With Cyclic Prefix and Conventional Detection

DMT with cyclic prefix is a popular multitone scheme that uses a rectangular prototype pulse. It is often referred to as OFDM with cyclic prefix. The efficient implementation of this scheme comprises at the transmitter an M-point IFFT followed by the insertion of a cyclic prefix of duration $\mu T = (N - M)T$. In this scheme, the number of subchannels is M and the symbol rate per subchannel is $1/T_0$ with $T_0 = NT$. At the receiver, the conventional detector disregards the cyclic prefix, it runs an M-point FFT, and finally it computes the decision statistics independently for the M subchannels. If the cyclic prefix is longer than the channel time dispersion, no ISI is present. However, if the channel is time variant over the duration of the FFT block, ICI is introduced [17], [18], [21]. If we assume Rayleigh faded channel taps with Jakes' Doppler spectrum, the BER performance of the conventional detector can be computed using the Gaussian approximation for the ICI. The computation of the bit error probability for BPSK–QPSK signaling on channel k yields

$$P_e(k) = \frac{1}{2}\left[1 - \sqrt{\frac{K_e E_{S,k}}{2(N_0 + I_k) + K_e E_{S,k}}}\right] \tag{44}$$

with $K_e = 2$ for BPSK and $K_e = 1$ for QPSK. In (44), the average useful signal power of subchannel k is

$$E_{S,k} = \frac{E_S}{MN} \sum_{p,p' \in \mathcal{P}} R_{p,p'} e^{j\frac{2\pi}{M}k(p'-p)} \times \sum_{n,n' \in \mathcal{K}} J_0\left(2\pi f_D T(n - n')\right) \tag{45}$$

while the power of the zero mean ICI is

$$I_k = -E_{S,k} + \frac{E_S}{N} \times \sum_{l=\{-1,0,1\}} \sum_{n,n' \in \mathcal{K}} \sum_{p,p' \in \mathcal{P}} \Big(R_{p,p'} e^{j\frac{2\pi}{M}k(p'-p)} \times J_0\left(2\pi f_D T(p - p' - lM)\right) \times \delta(n - n' - p + p' + lM) \Big) \tag{46}$$

where $R_{p,p'} = E[\alpha_p(iT)\alpha^*_{p'}(iT)]$, $\mathcal{K} = \{0, \ldots, M-1\}$, $\mathcal{P} = \{0, \ldots, 2N_P\}$, $M > \mu \geq 2N_P$. Therefore, we conclude that although conventional detection of DMT-CP is simple, it does not exploit the frequency diversity and suffers from the ICI introduced by the time-variant channel.

V. Numerical Results

In this section, we report several numerical results for the average and the distribution of the matched filter BER bound in various propagation conditions. The results are obtained assuming BPSK signaling and square-root-raised cosine filters in the DAC and ADC with a roll-off factor equal to 0.22. They apply to QPSK signaling by simply shifting the signal-to-noise ratio (SNR) by 3 dB. We choose the prototype pulse to be either rectangular in time (rect pulse), or rectangular in frequency (sinc pulse), or Gaussian (gauss pulse). The subcarrier spacing is minimal, i.e., $M = N$, $T_1 = T_0$.

In Fig. 2, we show the MFB BER complementary distribution as a function of the subcarrier index assuming $E_S/N_0 = 10$ dB and a Gaussian prototype pulse with normalized bandwidth $B = 0.33$. In the top figures, the channel is assumed to experience quasi-static (time-invariant over the prototype pulse duration) Rayleigh fading with a one-sided exponential power delay profile with root mean square (rms) delay spread $\tau_0 = 7.5$ T. The DAC–ADC filters are oversampled by a factor $K = 16$. Thus, the channel delay power profile reads $\phi_g(nT_c) = e^{-nT_c/\tau_0}(1 - e^{-T_c/\tau_0})/(1 - e^{-(\max(n)+1)T_c/\tau_0})$ with $n = 0, \ldots, \lceil 10\tau_0/T_c \rceil$ and $T_c = T/16$. This model is also known as the Chayat channel model [6]. As it can be seen in the top plots of Fig. 2, there is some variability in the BER distribution across the subchannels. The outermost channels exhibit worse BER distribution (in the plot, we assume $f_k = (k - \lfloor M/2 \rfloor)/T_1$). Further, as the number of subcarriers increases from 9 to 129, the frequency diversity gain diminishes as a result of subchannel bandwidth compression.

In the bottom plots of Fig. 2, we assume time-variant flat fading with Jakes' Doppler spectrum having normalized Doppler $f_D T = 0.01$. The plots show that the BER distribution is the same across the subchannels. Now, as the number of subcarriers increases, the distribution of the BER improves as the consequence of increased time-diversity exploitation.

From Figs. 3–9, we consider the 3GPP-ITU channel models with Jakes' Doppler spectrum whose power delay profile is shown in Table I. These channel models have been extensively used to evaluate the performance of 3G systems. We consider transmission bandwidths $W = 1/T$ equal to 24.3 kHz, 270.83 kHz, and 3.84 MHz. They correspond, respectively, to those of the IS-136, the Global System for Mobile Communications/Enhanced Data rates for Global Evolution (GSM/EDGE), and the Universal Mobile Telecommunications System (UMTS). They are representative of a narrowband system, a moderate narrowband system, and a wideband system. The plots are obtained with the numerical method described in Section III-A. The number of nodes w is set to 64, and we choose $c = 0.25$, which yields excellent accuracy.

[4]This can be proved as follows. For $M = N$ tending to infinity, the characteristic function of the squared distance converges to $\lim_{N=M\to\infty}(M/(M - jbD_e))^M = e^{jbD_e}$. That is, it converges in characteristic function, therefore, also in distribution, to the constant D_e.

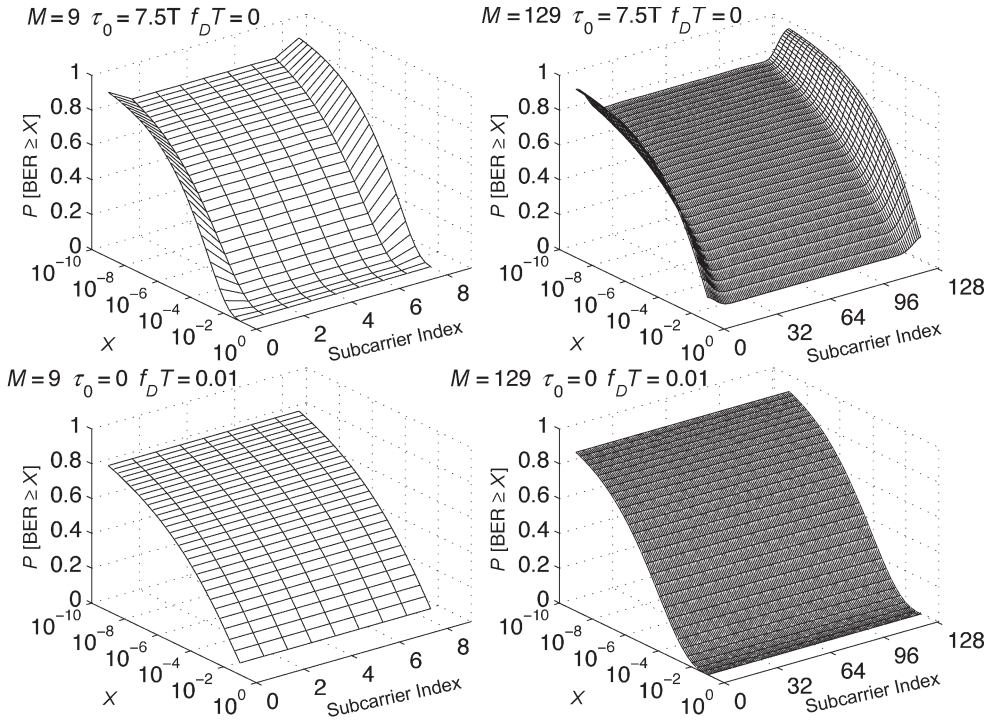

Fig. 2. MFB BER complementary distribution as a function of the subcarrier index with $E_S/N_0 = 10$ dB and Gaussian subchannel pulse. Frequency-selective Rayleigh fading channel with exponential power delay profile with delay spread τ_0 (top plots). Flat Rayleigh fading channel with Jakes' Doppler spectrum (bottom plots).

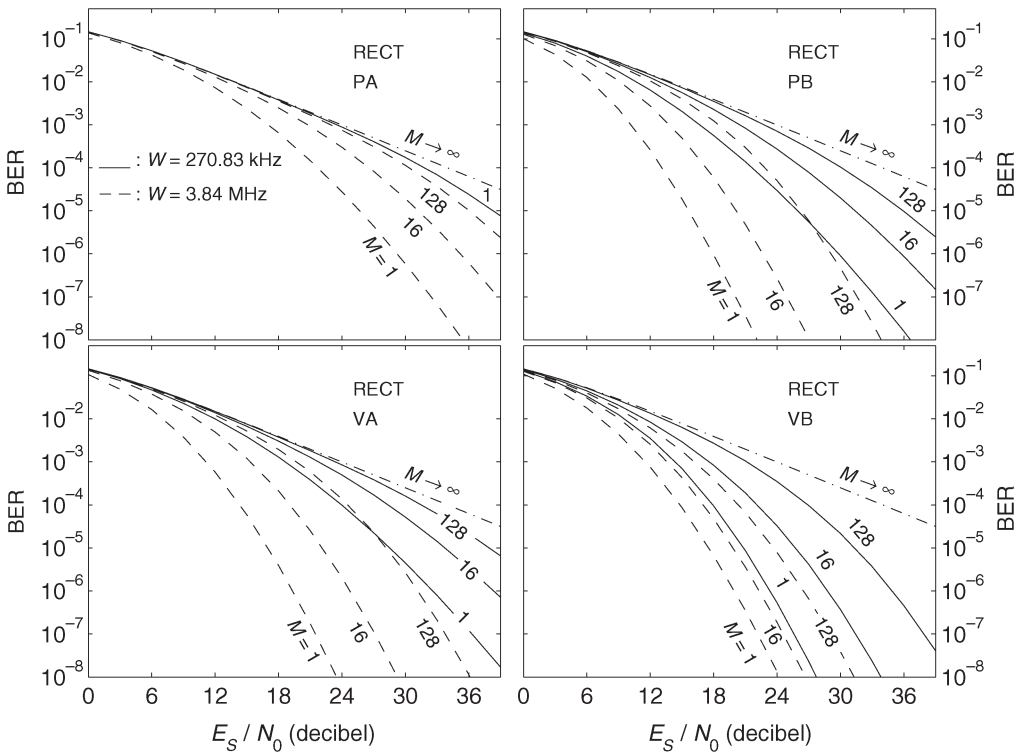

Fig. 3. Average MFB BER with rect subchannel pulse in ITU channels with quasi-static Rayleigh fading. Solid curves correspond to a transmission bandwidth $W = 270.83$ kHz, dashed curves to $W = 3.84$ MHz. Number of subchannels $M = 1, 16, 128, \infty$.

In Figs. 3–5, the channel is assumed quasi-static, i.e., $f_DT = 0$. We plot the average MFB BER, i.e., averaged over the subchannels, as a function of the SNR. We use rect subchannel pulses in Fig. 3, sinc pulses in Fig. 4, and gauss pulses with $B = 0.33$ in Fig. 5. This is to show how the subchannel pulse and the number of subcarriers affect the frequency diversity exploitation. As we increase the number of subcarriers, the diversity gain decreases, and in the limit $M \to \infty$, the average

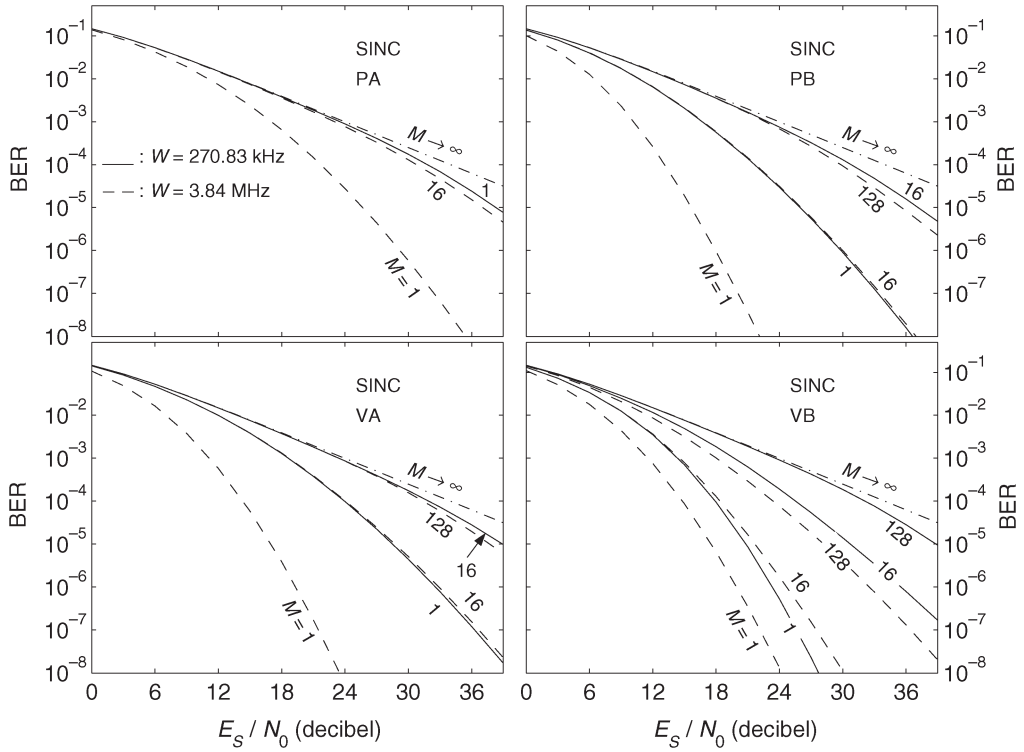

Fig. 4. Average MFB BER with sinc subchannel pulse in ITU channels with quasi-static Rayleigh fading. Solid curves correspond to a transmission bandwidth $W = 270.83$ kHz, dashed curves to $W = 3.84$ MHz. Number of subchannels $M = 1, 16, 128, \infty$.

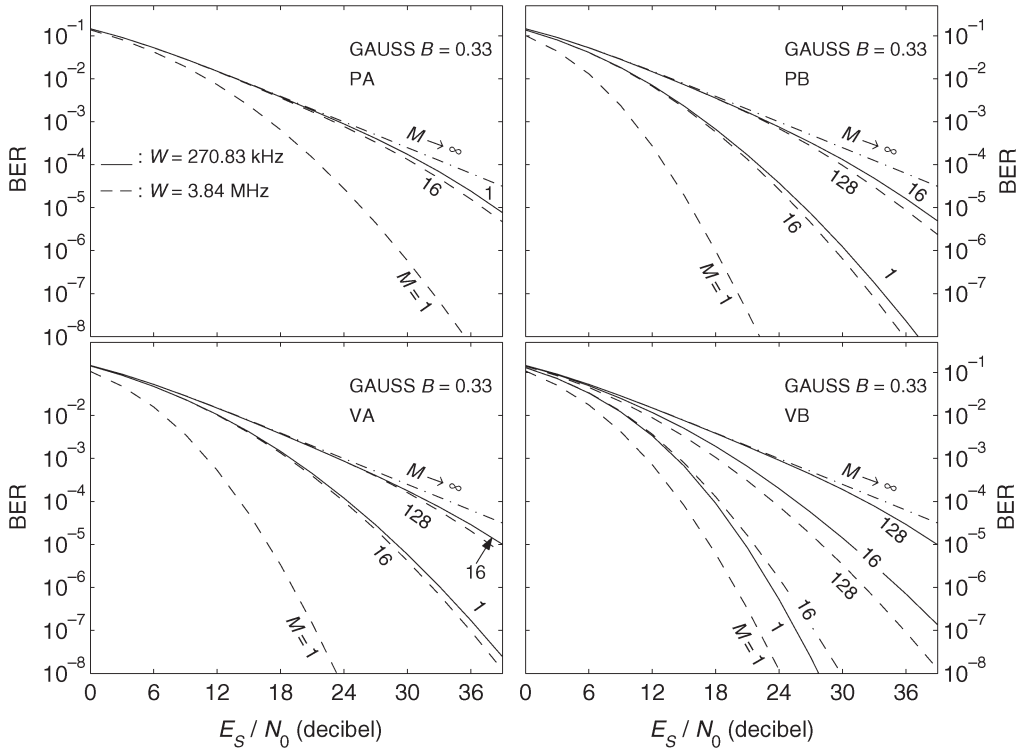

Fig. 5. Average MFB BER with gauss subchannel pulse in ITU channels with quasi-static Rayleigh fading. Solid curves correspond to a transmission bandwidth $W = 270.83$ kHz, dashed curves to $W = 3.84$ MHz. Number of subchannels $M = 1, 16, 128, \infty$.

BER for all the cases that we consider is practically identical to that of single carrier BPSK in flat fading. For $M = 1$ (single carrier modulation), the frequency diversity exploitation is maximized at the expense of receiver complexity. Further, note that the rect pulse yields the best performance. This is because, for a given number of subcarriers, it has a larger bandwidth than the gauss and the sinc pulse. The performance with gauss pulses is slightly better than with sinc pulses. Finally, the performance

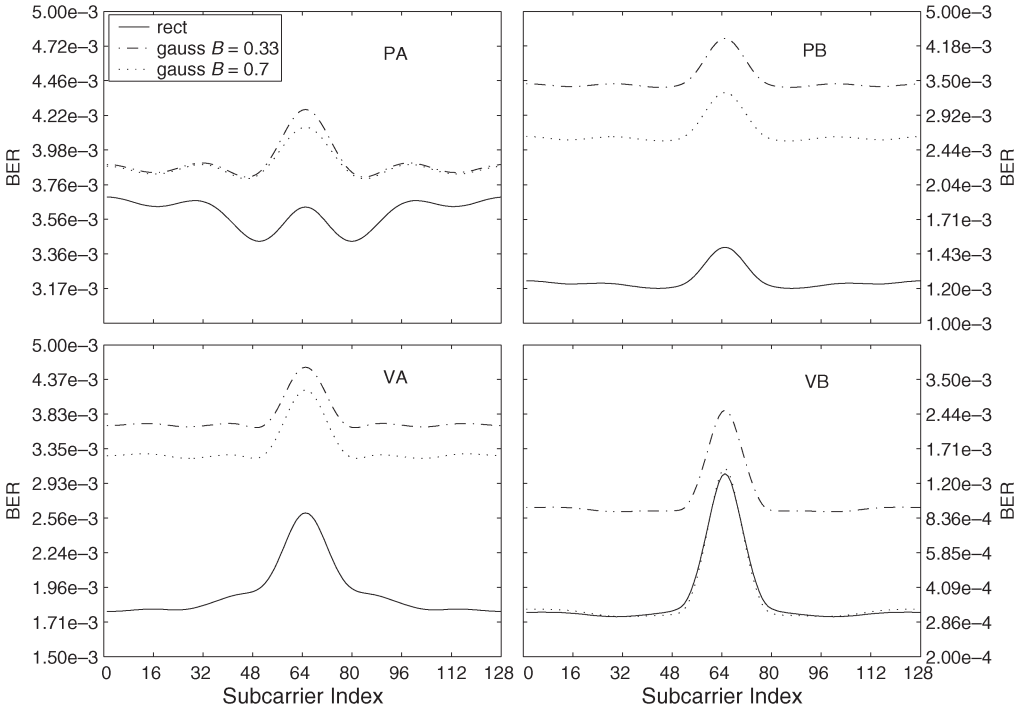

Fig. 6. MFB BER as a function of subcarrier index with gauss and rect subchannel pulse in ITU channels with quasi-static Rayleigh fading assuming a transmission bandwidth $W = 3.84$ MHz and $E_S/N_0 = 18$ dB.

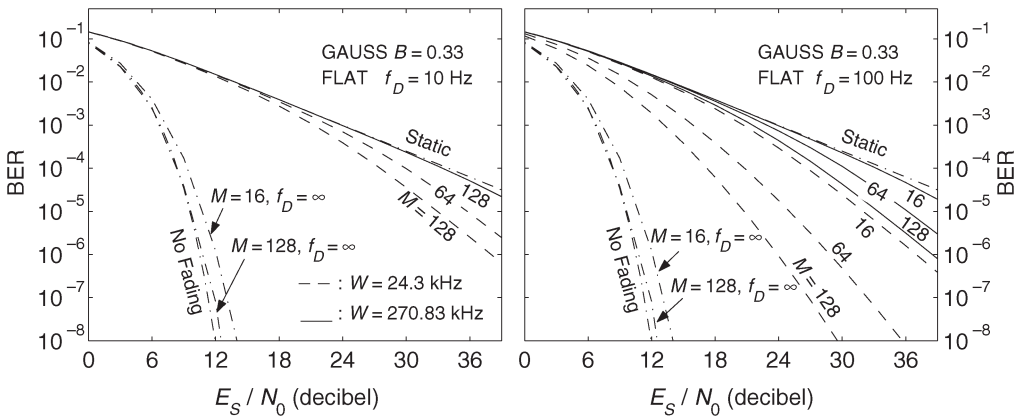

Fig. 7. Average MFB BER with gauss subchannel pulse in flat Rayleigh fading with Jakes' Doppler spectrum and $f_D = 10$, 100 Hz. Solid curves correspond to a transmission bandwidth $W = 270.83$ kHz, dashed curves to $W = 24.3$ kHz. Number of subchannels $M = 16$, 64, 128. Curves labeled with no fading correspond to BPSK in AWGN, curves labeled with static correspond to BPSK in quasi-static flat fading.

for the class B channels is in general better than for the class A channels since class B channels have a larger delay spread. It should be noted that from a detection complexity standpoint, the gauss pulse is a good option because of its time/frequency concentrated shape.

In Fig. 6, we plot the MFB BER as a function of the subchannel index assuming an SNR of 18 dB, $W = 3.84$ MHz, and $M = 128$ subcarriers. The subcarriers are chosen to be $f_k = k/T_1$. As can be seen, there is some performance variation across the subchannels although it is not deep. Again, with rect pulses, the performance is better; however, as we increase B to 0.7, the performance with gauss pulses improves since this translates into a subchannel bandwidth expansion. As we explained before, the variation of the BER performance across subchannels is a function of the channel tap correlation. Since the ADC filter is a Nyquist pulse, the T-spaced channel taps exhibit some correlation only for values of T that are not integer multiples of the time resolution of the ITU profiles, i.e., $T_c = 10$ ns.

In Figs. 7 and 8, we consider a time-variant flat-fading channel. This is to illustrate the effect of Doppler as a function of the subchannel pulse and the number of subcarriers. As a reference, we also report the BER of BPSK modulation in AWGN (no fading) and in quasi-static Rayleigh fading.

In Fig. 7, we deploy a Gaussian pulse with $B = 0.33$ and assume transmission bandwidths of $W = 24.3$ kHz and $W = 270.83$ kHz. In general, performance improves as the number of subcarriers increases since this corresponds to a pulse duration

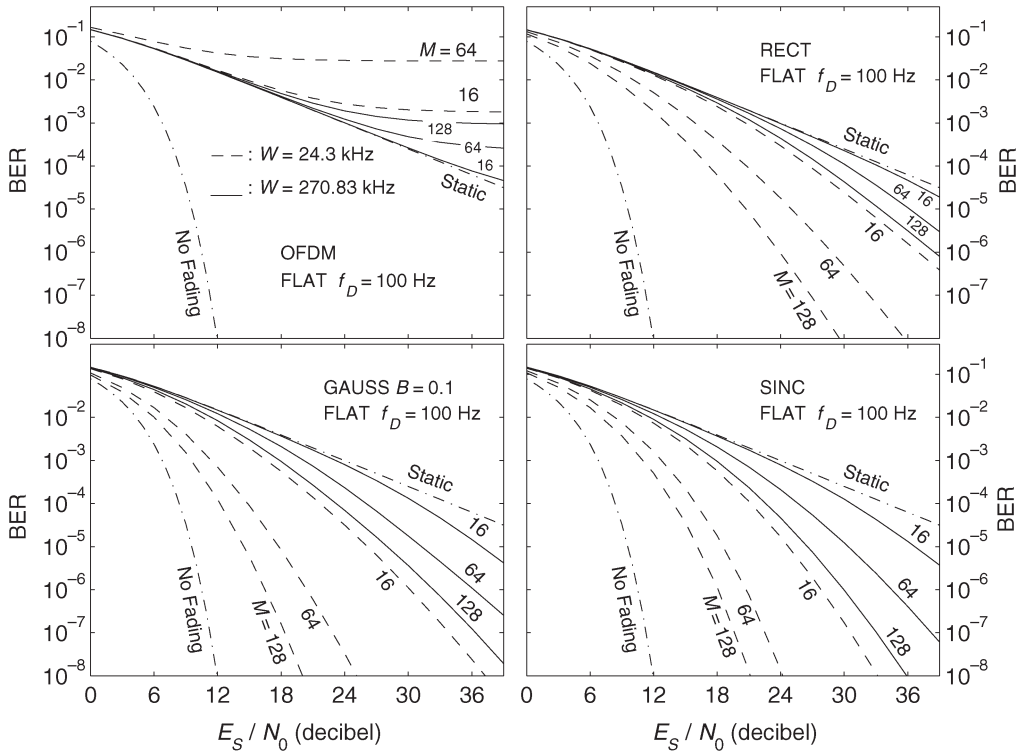

Fig. 8. Average BER in flat Rayleigh fading with Jakes' Doppler spectrum and $f_D = 100$ Hz. OFDM with conventional detection and MFB for rect pulse, gauss pulse, and sinc pulse. Solid curves correspond to a transmission bandwidth $W = 270.83$ kHz, dashed curves to $W = 24.3$ kHz. Number of subchannels $M = 16, 64, 128$. Curves labeled with no fading correspond to BPSK in AWGN, while curves labeled with static correspond to BPSK in flat fading.

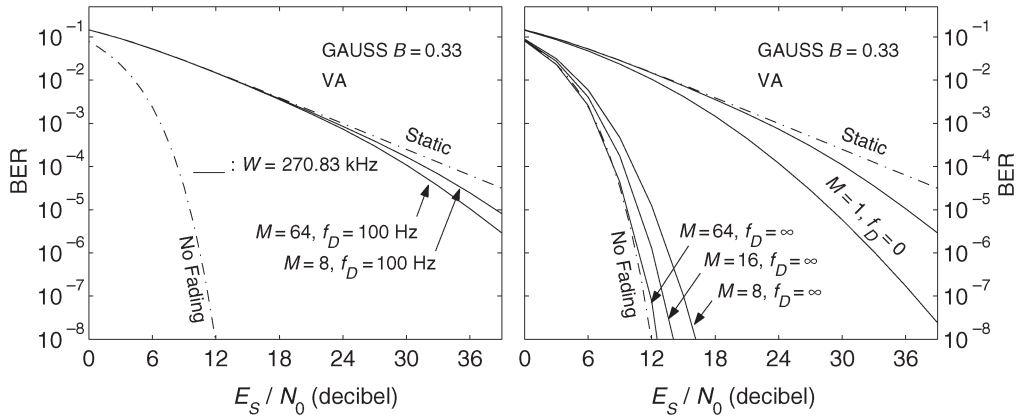

Fig. 9. Average MFB BER with gauss subchannel pulse in time–frequency selective channel: Vehicular A ITU channel with fading having Jakes' Doppler spectrum with $f_D = 100, \infty$ Hz. Transmission bandwidth $W = 270.83$ kHz. Curves labeled with no fading correspond to BPSK in AWGN, while curves labeled with static correspond to BPSK in flat fading.

TABLE I
3GPP-ITU POWER DELAY CHANNEL PROFILES

PA PEDESTRIAN A		PB PEDESTRIAN B		VA VEHICULAR A		VB VEHICULAR B	
Delay (nanosecond)	Power (decibel)	Delay (nanosecond)	Power (decibel)	Delay (nanosecond)	Power (decibel)	Delay (nanosecond)	Power (decibel)
0	0	0	0	0	0	0	-2.5
110	-9.7	200	-0.9	310	-1.0	300	0
190	-19.2	800	-4.9	710	-9.0	8900	-12.8
410	-22.8	1200	-8.0	1090	-10.0	12900	-10.0
-	-	2300	-7.8	1730	-15.0	17100	-25.2
-	-	3700	-23.9	2510	-20.0	20000	-16.0

expansion. Further, the time diversity effect is more evident in a narrowband context, i.e., with $W = 24.3$ kHz, but it is not negligible even with $W = 270.83$ kHz. It should be noted that for nontime-sensitive applications, we could combine multitone modulation with interleaving. That is, we could deploy symbol interleaving at the output of the multitone modulator. This would have the effect of decorrelating the channel. Thus, the multitone transform would yield higher time-diversity gains. If we look at the curves of Fig. 7 that correspond to a Doppler tending to infinity (ergodic channel), we can see that the BER approaches that of BPSK in AWGN (curves labeled with no fading).

In Fig. 8, we plot the performance of OFDM with conventional detection and the MFB performance with rect, gauss, and sinc pulses. No cyclic prefix is added here since flat fading is considered. OFDM with conventional detection exhibits high error floors that increase as the number of subcarriers increases. The best performance is achieved with sinc pulses. Gaussian pulses with $B = 0.1$ exhibit near sinc pulse performance.

Finally, in Fig. 9, we evaluate the performance for a joint time–frequency selective channel. We use a Gaussian subchannel pulse with $W = 270.83$ kHz and with the ITU vehicular A profile. If we compare the results in Fig. 9 with those in Figs. 5 and 7, we see that with $f_D = 100$ Hz there is some joint frequency and temporal diversity gain that is available by increasing the number of carriers to 16. However, this flattens out with 64 carriers since we start losing the frequency diversity gain. If the channel is fully temporally uncorrelated, then we can quickly approach the performance in AWGN (with no fading) by increasing the number of subcarriers to 64. In other words, we are better off exploiting the temporal diversity by increasing the number of subcarriers rather than the frequency diversity by deploying single carrier modulation.

VI. Conclusion

In this paper, we have studied the performance limits for FMT over time-variant frequency-selective fading channels through the analysis of the matched filter bound. We have shown that the time and frequency selectivity of the channel introduces ICI and ISI components that need to be counteracted with some form of equalization. We have reviewed the optimal ML detector and have shown that its complexity (related to the number of states in the Viterbi algorithm) is a function of the channel and the FMT modulator design parameters (prototype pulse and number of tones). To minimize the amount of ICI and ISI, it is desirable to use time- and frequency-concentrated pulses, e.g., Gaussian-shaped pulses. In the absence of ICI, the detector simplifies into a bank of ML detectors that operate independently over each subchannel. In quasi-static fading, an increase in the number of tones translates into a lower ISI exhibited by each subchannel. As a result, the exponential decrease in the number of states of each Viterbi detector exceeds the linear increase in the number of required detectors, which can yield a lower overall complexity. In fast time-variant fading, an increase in the number of tones can lead to a higher detection complexity. Thus, in general, the number of tones and prototype pulse is chosen to tradeoff between complexity and performance. Further, simplified detection algorithms can be developed. A possible approach is based on the deployment of a reduced state Viterbi algorithm combined with iterative detection that performs sequential interference cancellation [21]–[24]. Other simplified equalization schemes are described in [3].

With optimal detection, both the channel frequency and the temporal diversity can be exploited. To understand how the FMT modulator design parameters (prototype pulse and number of tones) impact performance, we have studied the matched filter bound error rate. The MFB yields a lower bound on the BER. It is a useful tool that allows for an analytical treatment of the diversity effect on performance as a function of the channel time and frequency selectivity [1], [8], [11], [13]. The MFB analysis reveals that multitone modulation can be interpreted as a diversity transform. In general, for a fixed transmission rate, an increase in the number of subcarriers translates into diminished frequency diversity gains, but into augmented time diversity gains. Therefore, from a pure performance perspective, optimal detection of multitone modulation allows for the diversity exploitation of the channel temporal selectivity that is, in general, exhibited in narrowband transmissions. On the contrary, wideband channels offer frequency selectivity whose diversity exploitation can be maximized with optimal detection of single carrier modulation. For a fixed number of tones, the prototype pulse shape also has an impact on performance. For instance, narrow bandwidth subchannel pulses yield better performance in time-selective fading than in frequency-selective fading. We note that the above conclusions are based on the analysis of the MFB performance of optimal detection. Further studies are required to characterize the performance of simplified/suboptimal equalization algorithms. Several simulation results for the more general multiuser system scenario in [21]–[24], [26] show that near MFB performance is achievable by deploying multitone detection schemes that are based on iterative interference cancellation techniques.

We have also briefly reviewed the performance of uncoded DMT modulation with cyclic prefix (OFDM). The conventional detector has an unbeatable simplicity but is suboptimal: it is unable to exploit the frequency diversity and cope with fast time-variant channels. It should be noted that sharp performance improvements can be obtained with channel coding across the OFDM subchannels [27], [30]. Channel coding is expected to be beneficial to FMT as well. The effect of coding can be studied by evaluating the squared distance (26) and the PEP (27) for error events of length larger than one symbol that are associated with code word pairs. Further, if bit-interleaved codes are used, we can treat the FMT system as a serially concatenated coded system and run decoding in a turbo-like fashion via iterative FMT equalization and channel decoding as described in [24] and [25].

Appendix A
Distribution of Normal Quadratic Forms

Let us consider the quadratic form $\Lambda = \boldsymbol{\alpha}^{\mathrm{H}}\mathbf{G}\boldsymbol{\alpha}$, where $\boldsymbol{\alpha}$ is a vector of circularly complex Gaussian random variables

with mean $\mathbf{m}$ and covariance $\mathbf{K}=\mathbf{R}-\mathbf{m}\mathbf{m}^{\mathrm{H}}$ while $\mathbf{G}$ is an Hermitian matrix of size N. Let $\mathbf{C}\mathbf{C}^{\mathrm{H}}=\mathbf{K}$ be the Cholesky factorization of $\mathbf{K}$ (assumed positive definite) and $\mathbf{U}$ be the unitary eigenvector matrix that diagonalizes $\mathbf{C}^{\mathrm{H}}\mathbf{G}\mathbf{C}$, i.e., $\mathbf{\Gamma}=\mathbf{U}\mathbf{C}^{\mathrm{H}}\mathbf{G}\mathbf{C}\mathbf{U}^{-1}=\mathrm{diag}\{\lambda_1,\ldots,\lambda_N\}$ [9], [16]. Then, we can write $\Lambda=\boldsymbol{\beta}^{\mathrm{H}}\mathbf{U}\mathbf{C}^{\mathrm{H}}\mathbf{G}\mathbf{C}\mathbf{U}^{-1}\boldsymbol{\beta}=\boldsymbol{\beta}^{\mathrm{H}}\mathbf{\Gamma}\boldsymbol{\beta}=\sum_{i=1}^{N}\lambda_i|\beta_i|^2$, where $\boldsymbol{\beta}=\mathbf{U}\mathbf{C}^{-1}\boldsymbol{\alpha}$ is a vector of independent Gaussian random variables with unit variance and mean $\mathbf{m}_\beta=\mathbf{U}\mathbf{C}^{-1}\mathbf{m}$.

It is interesting to note that the eigenvalues of $\mathbf{C}^{\mathrm{H}}\mathbf{G}\mathbf{C}$ are the same as the eigenvalues of $\mathbf{K}\mathbf{G}$. In fact, if $\mathbf{C}^{\mathrm{H}}\mathbf{G}\mathbf{C}\boldsymbol{\nu}_k=\lambda_k\boldsymbol{\nu}_k$, then $\mathbf{C}\mathbf{C}^{\mathrm{H}}\mathbf{G}\mathbf{C}\boldsymbol{\nu}_k=\lambda_k\mathbf{C}\boldsymbol{\nu}_k$ and finally $\mathbf{K}\mathbf{G}\mathbf{C}\boldsymbol{\nu}_k=\lambda_k\mathbf{C}\boldsymbol{\nu}_k$, where $\mathbf{C}\boldsymbol{\nu}_k$ is the kth eigenvector associated with the eigenvalue λ_k of $\mathbf{K}\mathbf{G}$. Therefore, we just need to determine the eigenvalues of $\mathbf{K}\mathbf{G}$ without computing the Cholesky factorization of $\mathbf{K}$.

Herein, we consider the case of central and positive semidefinite quadratic form, i.e., $\mathbf{m}=\mathbf{0}$, $\mathbf{K}=\mathbf{R}$, and $\lambda_k\geq 0$. In such a case, the pdf of Λ can be found via the partial fraction expansion of the characteristic function [5], [8], [15]. Assuming N' distinct eigenvalues each with multiplicity m_k, we can rewrite $\Lambda=\sum_{i=1}^{N'}\sum_{k=1}^{m_i}\lambda_i|\beta_{i,k}|^2=\sum_{i=1}^{N'}\gamma_i$, with $\gamma_i=\lambda_i\sum_{k=1}^{m_i}|\beta_{i,k}|^2$ being independent and Erlang-distributed random variables with order m_i and mean $\lambda_i m_i$. Their characteristic function reads $\psi_\gamma(a)=E[e^{j\gamma a}]=(1-j\lambda_i a)^{-m_i}$ [14]. Therefore, the characteristic function of Λ is $\psi_\Lambda(b)=\prod_{i=1}^{N'}(1-j\lambda_i b)^{-m_i}=\sum_{i=1}^{N'}\sum_{k=1}^{m_i}A_{i,k}(1-j\lambda_i b)^{-k}$, where we have used the partial fraction expansion with coefficients given by (34). Now, the pdf of Λ is obtained from the characteristic function as $p_\Lambda(a)=1/(2\pi)\int_{-\infty}^{\infty}\psi_\Lambda(b)e^{-jab}\mathrm{d}b$, which yields (32), while the cumulative distribution function (cdf) as $F_\Lambda(a)=\int_0^a p_\Lambda(b)\mathrm{d}b$, which yields (33).

Appendix B
Gauss–Chebyshev Numerical Quadrature Method

In this appendix, we describe a numerical method to evaluate the average probability of error as reported in (38) (see also [19]). Let us define the random variable $\Delta=\xi-\nu^2$, where ν is zero-mean unit-variance Gaussian and ξ is a nonnegative random variable independent of ν. Then, we can write

$$E\left[Q(\sqrt{\xi})\right]=P[\nu>\sqrt{\xi}]=\frac{1}{2}P[\nu^2>\xi]=\frac{1}{2}P[\Delta<0]. \tag{47}$$

Note that the result in (47) differs by a factor 1/2 from the one erroneously reported in [19]. Then, if $\Phi_\Delta(s)$ is the moment generating function of Δ, through the Laplace inversion formula we obtain its pdf $p_\Delta(a)=1/(2\pi j)\int_{c-j\infty}^{c+j\infty}\Phi_\Delta(s)e^{-as}\mathrm{d}s$, with c in the region of convergence of $\Phi_\Delta(s)$. Consequently

$$E\left[Q(\sqrt{\xi})\right]=\frac{1}{2}P[\Delta<0]=\frac{1}{4\pi j}\int_{c-j\infty}^{c+j\infty}\frac{\Phi_\Delta(s)}{s}\mathrm{d}s. \tag{48}$$

With the change of variable $s=c+jc\sqrt{1-x^2}/x$, the integral in (48) can be manipulated to obtain

$$P[\Delta<0]=\frac{1}{2\pi}\int_{-1}^{1}\left[\mathrm{Re}\left\{\Phi_\Delta\left(c+jc\frac{\sqrt{1-x^2}}{x}\right)\right\}+\frac{\sqrt{1-x^2}}{x}\mathrm{Im}\left\{\Phi_\Delta\left(c+jc\frac{\sqrt{1-x^2}}{x}\right)\right\}\right]\frac{\mathrm{d}x}{\sqrt{1-x^2}}. \tag{49}$$

If we use the Gauss–Chebyshev numerical integration formula $\int_{-1}^{1}f(x)/\sqrt{1-x^2}\mathrm{d}x\cong\pi/w\sum_{n=1}^{w}f(\cos((2n-1)\pi/2/w))$, we obtain (38).

We can proceed by noting that the moment generating function that is required in (38) can be written as $\Phi_\Delta(s)=\Phi_\xi(s)(1-2s)^{-1/2}$. Further, in our context, we want to evaluate $P_{e,\mathrm{MFB}}(k)=E[Q(\sqrt{\xi})]$ with ξ from (29)

$$\xi=\frac{d^2_{\mathrm{MFB}}(k,l)}{2N_0}=\frac{D_e}{2N_0}\boldsymbol{\alpha}^{\mathrm{H}}\mathbf{W}_k^{\mathrm{H}}\mathbf{G}\mathbf{W}_k\boldsymbol{\alpha}. \tag{50}$$

The moment generating function $\Phi_\xi(s)=E[e^{-s\xi}]$ can be computed in closed form. Since $\boldsymbol{\alpha}$ is Gaussian with mean $\mathbf{m}$ and covariance matrix $\mathbf{K}=\mathbf{R}-\mathbf{m}\mathbf{m}^{\mathrm{H}}$, following [16, Appendix B], we obtain

$$\begin{aligned}\Phi_\xi(s)&=\frac{e^{-s\mathbf{m}^{\mathrm{H}}\mathbf{W}_k^{\mathrm{H}}\mathbf{G}\mathbf{W}_k\left(\frac{2N_0}{D_e}\mathbf{I}+s\mathbf{K}\mathbf{W}_k^{\mathrm{H}}\mathbf{G}\mathbf{W}_k\right)^{-1}\mathbf{m}}}{\left|\mathbf{I}+s\frac{D_e}{2N_0}\mathbf{K}\mathbf{W}_k^{\mathrm{H}}\mathbf{G}\mathbf{W}_k\right|}\\&\overset{\mathbf{m}=\mathbf{0}}{\Rightarrow}=\left|\mathbf{I}+s\frac{D_e}{2N_0}\mathbf{R}\mathbf{W}_k^{\mathrm{H}}\mathbf{G}\mathbf{W}_k\right|^{-1}\\&=\prod_i\left(1+s\frac{\lambda_i}{2N_0}\right)^{-1}\end{aligned} \tag{51}$$

where $\mathbf{I}$ denotes the identity matrix and λ_i are the eigenvalues of $D_e\mathbf{R}\mathbf{W}_k^{\mathrm{H}}\mathbf{G}\mathbf{W}_k$. Thus, the method is easily applicable to the case of $\boldsymbol{\alpha}$ having nonzero mean, i.e., Ricean fading. For the Rayleigh fading case, setting $\mathbf{m}=\mathbf{0}$, $s=c(1+j\tau_n)$ and using (38) yields the final result.

Acknowledgment

The author wishes to thank Dr. R. Bernardini for helpful discussions on the efficient implementation of the numerical methods herein described.

References

[1] N. J. Baas and D. P. Taylor, "Matched filter bounds for wireless communication over Rayleigh fading dispersive channels," *IEEE Trans. Commun.*, vol. 49, no. 9, pp. 1525–1528, Sep. 2001.

[2] P. A. Bello, "Characterization of randomly time-variant linear channels," *IEEE Trans. Commun. Syst.*, vol. COMM-11, no. 4, pp. 360–393, Dec. 1963.

[3] N. Benvenuto, S. Tomasin, and L. Tomba, "Equalization methods in DMT and FMT systems for broadband wireless communications," *IEEE Trans. Commun.*, vol. 50, no. 9, pp. 1413–1418, Sep. 2002.

[4] J. A. C. Bingham, "Multicarrier modulation for data transmission: An idea whose time has come," *IEEE Commun. Mag.*, vol. 28, no. 5, pp. 5–14, May 1990.

[5] J. K. Cavers and P. Ho, "Analysis of the error performance of trellis-coded modulations in Rayleigh fading channels," *IEEE Trans. Commun.*, vol. 40, no. 1, pp. 74–83, Jan. 1992.
[6] N. Chayat, *Tentative criteria for comparison of modulation methods*, IEEE P802.11-97/96, Sep 1997.
[7] G. Cherubini, E. Eleftheriou, S. Olcer, and J. M. Cioffi, "Filter bank modulation techniques for very high-speed digital subscriber lines," *IEEE Commun. Mag.*, vol. 38, no. 5, pp. 98–104, May 2000.
[8] M. V. Clark, L. J. Greenstein, W. K. Kennedy, and M. Shafi, "Matched filter performance bounds for diversity combining receivers in digital mobile radio," *IEEE Trans. Veh. Technol.*, vol. 41, no. 4, pp. 356–362, Nov. 1992.
[9] R. A. Horn and C. R. Johnson, *Matrix Analysis*. Cambridge, U.K.: Cambridge Univ. Press, 1988.
[10] W. C. Jakes, *Microwave Mobile Communications*. New York: Wiley, 1974.
[11] T. Hunziker and D. Dahlhaus, "Bounds on matched filter performance in doubly dispersive Gaussian WSSU channels," *Electron. Lett.*, vol. 37, no. 6, pp. 383–384, Mar. 2001.
[12] "Universal Mobile Telecommunication System (UMTS); Selection procedures for the choice of radio transmission technologies for the UMTS," ETSI, Sophia-Antipolis, France, TR 101.112, 1998.
[13] J. E. Mazo, "Exact matched filter bound for two-beam Rayleigh fading," *IEEE Trans. Commun.*, vol. 39, no. 7, pp. 1027–1030, Jul. 1991.
[14] J. G. Proakis, *Digital Communications*, 3rd ed. New York: McGraw-Hill, 1995.
[15] C. Schlegel, "Error probability calculation for multibeam Rayleigh channels," *IEEE Trans. Commun.*, vol. 44, no. 3, pp. 290–293, Mar. 1996.
[16] M. Schwartz, W. R. Bennet, and S. Stein, *Communication Systems and Techniques*. New York: McGraw-Hill, 1966.
[17] M. Speth, S. A. Fetchel, G. Fock, and H. Meyr, "Optimum receiver design for wireless broad-band systems using OFDM—Part I," *IEEE Trans. Commun.*, vol. 47, no. 11, pp. 1668–1677, Nov. 1999.
[18] G. L. Stuber, *Principles of Mobile Communications*, 1st ed. Boston, MA: Kluwer, 1996.
[19] G. Taricco and E. Biglieri, "Exact pairwise error probability of space–time codes," *IEEE Trans. Inf. Theory*, vol. 48, no. 2, pp. 510–513, Feb. 2002.
[20] V. Tarokh, N. Seshadri, and A. R. Calderbank, "Space–time codes for high data rate wireless communication: Performance criterion and code construction," *IEEE Trans. Inf. Theory*, vol. 44, no. 2, pp. 744–765, Mar. 1998.
[21] A. M. Tonello, "Multicarrier multiuser asynchronous communications," Doctor of research degree thesis, DEI-Dept. Elect. Eng., Univ. Padova, Padova, Italy, Dec. 2001.
[22] ——, "Multiuser detection and turbo multiuser decoding for asynchronous multitone multiple access systems," in *Proc. IEEE Vehicular Technology Conf. Fall*, Vancouver, BC, Canada, Sep. 2002, pp. 970–974.
[23] ——, "Multiuser detection/decoding in asynchronous multitone multiple access systems," in *Proc. IEEE Wireless Personal Multimedia Communications Symp.*, Honolulu, HI, Oct. 2002, pp. 1242–1246.
[24] ——, "Asynchronous multicarrier multiple access: Optimal and sub-optimal detection and decoding," *Bell Labs Tech. J.*, vol. 7, no. 3, pp. 191–217, Feb. 2003.
[25] ——, "MIMO MAP equalization and turbo decoding in interleaved space–time coded systems," *IEEE Trans. Commun.*, vol. 51, no. 2, pp. 155–160, Feb. 2003.
[26] A. M. Tonello and S. Pupolin, "Performance of single user detectors in multitone multiple access asynchronous communications," in *Proc. IEEE Vehicular Technology. Conf. Spring*, Birmingham, AL, May 2002, pp. 199–203.
[27] A. M. Tonello and R. Bernardini, "On the exploitation of the time–frequency diversity in coded OFDM," in *Proc. Wireless Personal Multimedia Communications Symp.*, Yokosuka, Japan, Oct. 19–22, 2003, vol. 2, pp. 193–197.
[28] G. Ungerboeck, "Adaptive maximum likelihood receiver for carrier-modulated data transmission systems," *IEEE Trans. Commun.*, vol. COMM-22, no. 5, pp. 624–636, May 1974.
[29] W. Van Etten, "Maximum likelihood receiver for multiple channel transmission systems," *IEEE Trans. Commun.*, vol. COMM-24, no. 2, pp. 276–283, Feb. 1976.
[30] Z. Wang and G. B. Giannakis, "Wireless multicarrier communications," *IEEE Signal Process. Mag.*, vol. 17, no. 3, pp. 29–48, May 2000.

Andrea M. Tonello (S'00–M'02) received the Doctor of Engineering degree in electronics (*cum laude*) in 1996 and the Doctor of Research degree in electronics and telecommunications in 2002 both from the University of Padova, Italy.

In February 1997, he was a Member of the Technical Staff of Bell Labs-Lucent Technologies where he worked on the development of baseband algorithms for cellular handsets first in Holmdel, NJ, and then within the Philips/Lucent Consumer Products Division in Piscataway, NJ. From September 1997 to December 2002, he was with the Bell Labs Advanced Wireless Technology Laboratory, Whippany, NJ. He was promoted in 2002 to Technical Manager and was appointed Managing Director of Bell Labs Italy. In January 2003, he joined the Department of Electrical, Mechanical, and Management Engineering (DIEGM) of the University of Udine, Udine, Italy, where he is currently an Assistant Professor. He has been involved in the standardization activity for the evolution of the IS-136 time division multiple access (TDMA) technology within Universal Wireless Communications Consortium/Telecommunications Industry Association (UWCC/TIA). His research interests include wireless and powerline communications. He is the author of several papers and patents.

Dr. Tonello received a Lucent Bell Labs Recognition of Excellence Award for his work on enhanced receiver techniques. He was a Committee Member of the 9th International Symposium on Powerline Communications (ISPLC 2005), April 2005, Vancouver, BC, Canada.